Supporting Information for:

The Dynamic Double Lattice of 1-Adamantaneselenolate Self-Assembled Monolayers on Au{111}

J. Nathan Hohman,[a,b] Moonhee Kim,[a] Björn Schüpbach,[c] Martin Kind,[c] John C. Thomas,[a] Andreas Terfort,*[c] and Paul S. Weiss*[a,b,d]

[a]California NanoSystems Institute and Department of Chemistry and Biochemistry, University of California, Los Angeles, Los Angeles, CA 90095, United States

[b]Department of Chemistry, The Pennsylvania State University, University Park, PA 16802, USA

[c]Institut für Anorganische und Analytische Chemie, Universität Frankfurt, Frankfurt, Germany 60438

[d]Department of Materials Science and Engineering, University of California, Los Angeles, Los Angeles, CA 90095, USA

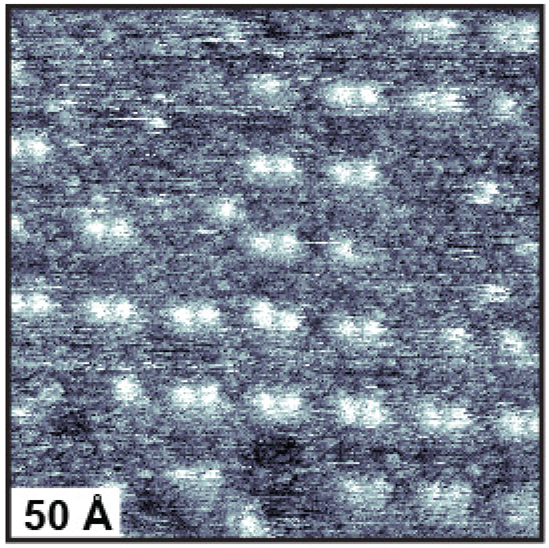

Figure S1: Unfiltered image of a dry-annealed 1-adamantaneselenolate SAM on Au{111} shown in Fig. 2B of the main text. Dry annealing at 70 °C triggers self-organization of the high-conductance molecules into a distinctive dimer structure; low-conductance molecules are not altered appreciably by annealing. Order is long range, and persists beyond defects in the dimer-pair lattice (described below). Molecules are dynamic and switch between high- and low-conductance states whether organized or randomly distributed. The 512 × 512 pixel STM image was collected at a sample bias of -1.0 V and 1 pA tunneling current.

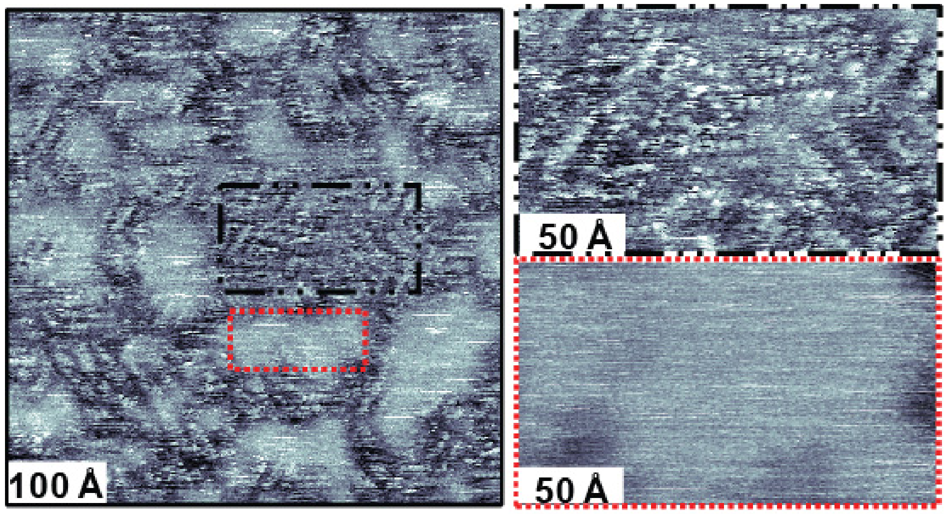

Figure S2: Annealing above 75 °C triggers a structural collapse of the monolayer; here the monolayer has been annealed at 85 °C. The expanded region in the black box is reminiscent of the missing-row phase observed in *n*-alkaneselenolate structures.[S1] The large, featureless islands (the example denoted by the red box is illustrative) are similar in absolute height to molecular rows, protruding by ~1.5 Å. The STM images were recorded at -1 V sample bias and 1 pA tunneling current.

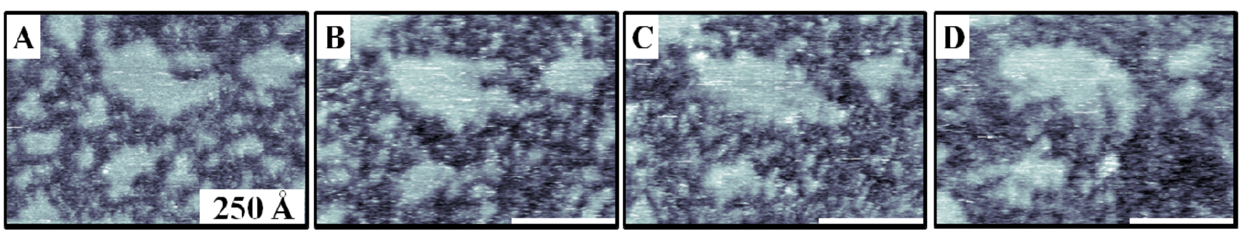

Figure S3: (A to D) Images collected at 30 min intervals revealing the dynamics of a 85 °C dry-annealed 1-adamantaneselenolate SAM on Au{111}, collected at a sample bias of -1.0 V and 10 pA tunneling current. Monitoring this region for two hours revealed changes in the morphology of the featureless island domains.

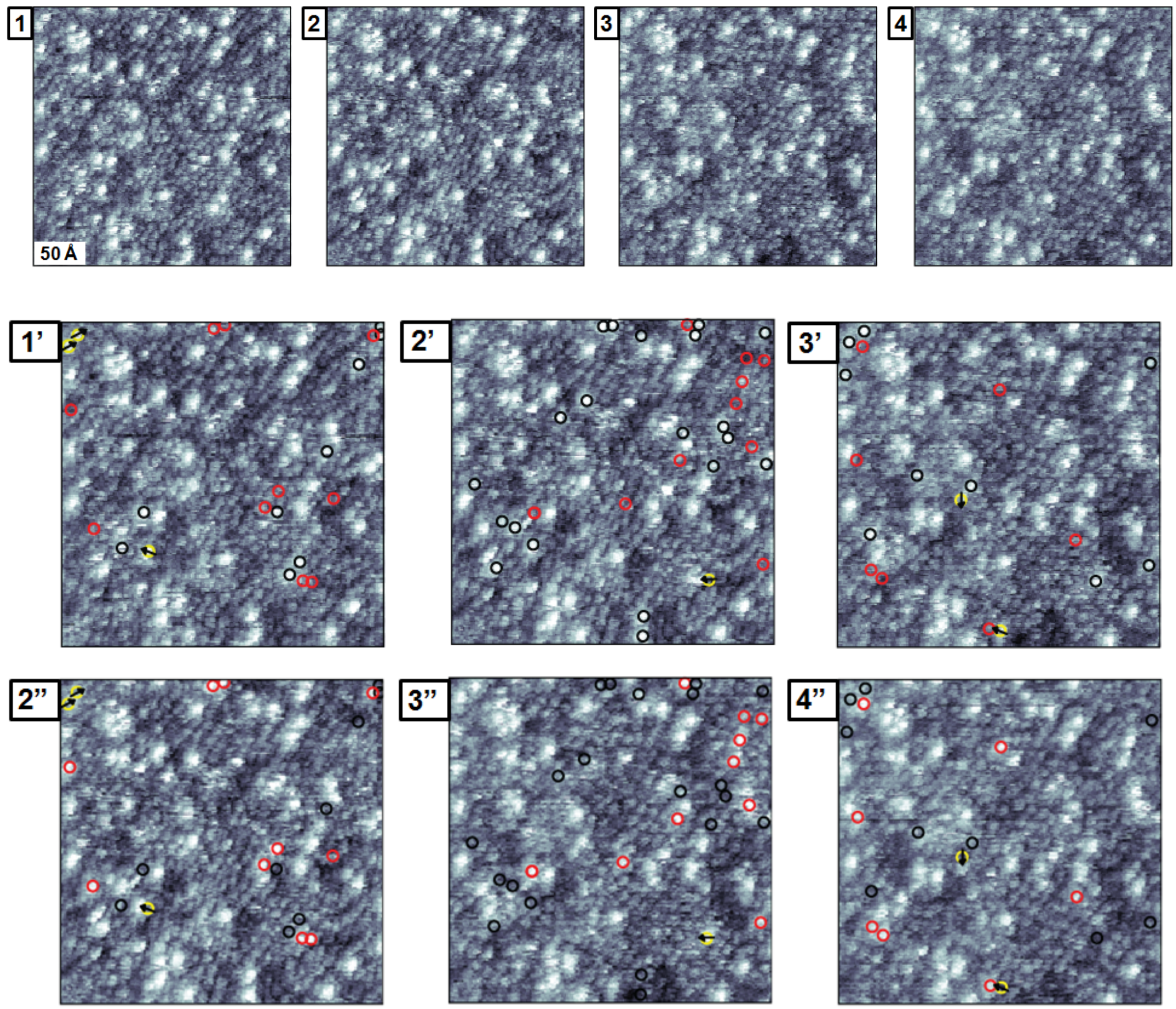

Figure S4: (1-4) Sequential scanning tunneling microscope images of an unannealed 1-adamantaneselenolate self-assembled monolayer with randomly distributed high-conductance molecules. Molecules switch between low- and high-conductance states faster than the imaging time (minutes). Each image pair (*e.g.*, 1’ *vs* 2”) details the dynamics of the sequence. Molecules with red circles switch to the high-conductance state in the next image, while molecules with black circles have switched to the low-conductance state. Molecules with yellow circles appear to shift to an adjacent position in the direction of the black arrows. Images were obtained at a sample bias of -1 V and 1 pA tunneling current.

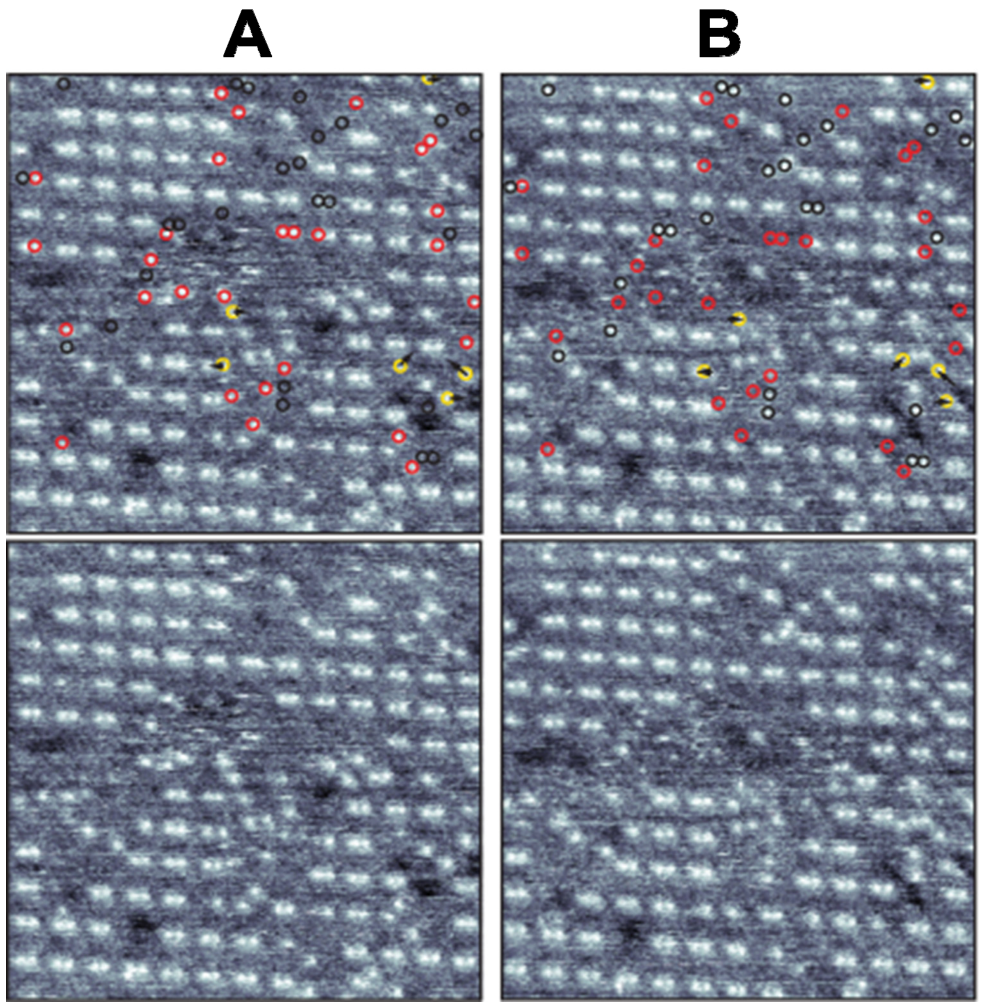

Figure S5: (A and B) Two sequential scanning tunneling microscope images annotated (top) and unanotated (bottom) of an annealed 1-adamantaneselenolate self-assembled monolayer in which high-conductance dimers are ordered. Molecules switch between low- and high-conductance states between images. There is a preference, but not a restriction, for dynamics at or adjacent to defect sites and in regions of disorder. Molecules with red circles switch to the low-conductance state in the subsequent image, while molecules with black circles have just switched to the high-conductance state in the image shown. Molecules bounded by the yellow circles appear to have moved to adjacent lattice positions, but may be due to two molecules in adjacent positions switching separately. Images were obtained at a sample bias of -1 V and 1 pA tunneling current.

Table S1: Wavenumbers (given in cm^{-1}) and assignments of the vibrational bands of 1-adamantaneselenol species along with the orientation of their transition dipole moments (TDMs). Calculated frequencies are scaled by a factor of 0.986.

No.	Vibrational Mode	TDM	Calc	Bulk	SAM (solution)	SAM (gas phase)
*					2958 m	2958 m
26	ν_{as} CH_2	⊥	3032	2926 m sh	2925 s sh	2924 s sh
25	ν_{as} CH_2	||	3015	2912 s sh	2914 vs	2914 vs
24	ν_s CH_2, ν CH	⊥	2998	2899 vs	2898 m sh	2900 m sh
23	ν_s CH_2	/	2971	2846 s	2852 m	2852 m
22	ν SeH	-	2314	2322 vw sh		
21	ν SeH			2299 w		
*						1739 w
*						1676 vw
20	δ_{bend} CH_2	||	1469	1470 w	1466 w	1468 w
19	δ_{bend} CH_2	/	1445	1452 m	1450 m	1448 m
18	δ_{bend} CH_2	/	1431	1427 w sh		
17	δ CC, τ CH_2, δ CH	⊥	1370	1363 vw		
16	γ CH_2, δ CH	⊥	1349	1342 m	1338 w	1338 w
15	γ CH_2, δ CH	/	1318	1311 w	1309 w	1311 w
14	δ CH, δ_{rock} CH_2	||	1304	1296 m	1290 m	1290 m
13	τ CH_2, ν CC	||	1292	1286 w sh		
12	δ CSe, τ CH_2, δ CH	⊥	1259	1255 w	1257 w	1255 w
11	τ CH_2, δ CH	/	1183	1180 vw		
10	γ CH_2, δ CH	⊥	1104	1101 m	1097 vw	1099 w
9	δ CCC, δ_{rock} CH	||	1037	1036 s	1028 m	1028 m
8	ν CSe, δ_{bend} CC, δ_{rock} CH_2	⊥	976	978 m		
7	ν CC, δ_{rock} CH_2	||	959	958 m	951 m	951 m
6	ν CSe, ν CC, δ_{bend} CSeH	||	815	825 m		
5	ν CC, δ_{bend} CSeH	||	809	808 w	806 vw	802 vw
4	ν CC	⊥	806	789 vw		
3	ν CC, δ_{bend} CSeH	||	760	766 w		
2	δ_{bend} CSeH	-	734	733 w		
1	ν CSe, δ CCC	||	673	675 m	671 w	671 w

*: assignment not possible, ν: stretch mode, as: asymmetric, s: symmetric, δ: deformation, bend: bending, τ: torsion, γ: wagging, rock: rocking, vs: very strong, s: strong, m: medium, w: weak, vw: very weak, sh: shoulder

Direction of the TDM: || completely or predominantly parallel to the Se-C axis, ⊥ completely or predominantly perpendicular to the Se-C axis, / neither parallel nor perpendicular to the Se-C axis, - either irrelevant or not ascertainable due to uncertainty of assignment.

Full Citation for Reference 116:

(116) Frisch, M. J.; Trucks, G. W.; Schlegel, H. B.; Scuseria, G. E.; Robb, M. A.; Cheeseman, J. R.; Scalmani, G.; Barone, V.; Mennucci, B.; Petersson, G. A.; Nakatsuji, H.; Caricato, M.; Li, X.; Hratchian, H. P.; Izmaylov, A. F.; Bloino, J.; Zheng, G.; Sonnenberg, J. L.; Hada, M.; Ehara, M.; Toyota, K.; Fukuda, R.; Hasegawa, J.; Ishida, M.; Nakajima, T.; Honda, Y.; Kitao, O.; Nakai, H.; Vreven, T.; Montgomery, Jr., J. A.; Peralta, J. E.; Ogliaro, F.; Bearpark, M.; Heyd, J. J.; Brothers, E.; Kudin, K. N.; Staroverov, V. N.; Kobayashi, R.; Normand, J.; Raghavachari, K.; Rendell, A.; Burant, J. C.; Iyengar, S. S.; Tomasi, J.; Cossi, M.; Rega, N.; Millam, N. J.; Klene, M.; Knox, J. E.; Cross, J. B.; Bakken, V.; Adamo, C.; Jaramillo, J.; Gomperts, R.; Stratmann, R. E.; Yazyev, O.; Austin, A. J.; Cammi, R.; Pomelli, C.; Ochterski, J. W.; Martin, R. L.; Morokuma, K.; Zakrzewski, V. G.; Voth, G. A.; Salvador, P.; Dannenberg, J. J.; Dapprich, S.; Daniels, A. D.; Farkas, Ö.; Foresman, J. B.; Ortiz, J. V.; Cioslowski, J.; Fox, D. J. Gaussian 09, Revision A.1, Gaussian, Inc., Wallingford CT, **2009**.

Reference

(S1) Monnell, J. D.; Stapleton, J. J.; Jackiw, J. J.; Dunbar, T.; Reinerth, W. A.; Dirk, S. M.; Tour, J. M.; Allara, D. L.; Weiss, P. S. *J. Phys. Chem. B* **2004**, *108*, 9834-9841.